International Journal of Naval Architecture and Ocean Engineering 12 (2020) 832–842

Contents lists available at ScienceDirect

International Journal of Naval Architecture and Ocean Engineering

journal homepage: http://www.journals.elsevier.com/international-journal-of-naval-architecture-and-ocean-engineering/

Spatial target path following and coordinated control of multiple UUVs

Xue Qi [a, *], Peng Xiang [b], Zhi-jun Cai [b]

[a] College of Information and Network Engineering, Anhui Science and Technology University, Fengyang, 233100, China
[b] School of Finance and Economics, Anhui Science and Technology University, Fengyang, 233100, China

ARTICLE INFO

Article history:
Received 20 December 2017
Received in revised form
26 September 2019
Accepted 11 November 2019

Keywords:
Underactuated underwater vehicle
Coordinated control
Path following
Spatial target

ABSTRACT

The coordination control of multiple Underactuated Underwater Vehicles (UUVs) moving in three dimensional space is investigated in this paper. The coordinated path following control task is decomposed into two sub tasks, that is, path following control and coordination control. In the spatial curve path following control task, path following error dynamics is build in the Serret-Frenet coordinate frame. The virtual reference object can be chosen freely on the desired spatial path. Considering the speed of the UUV, the line-of-sight navigation is introduced to help the path following errors quickly converge to zero. In the coordination control sub task, the communication topology of multiple UUVs is described by the graph theory. The speed of each UUV is adjusted to achieve the coordination. The path following system and the coordination control system are viewed as the feedback connection system. Input-to-state stable of the coordinated path following system can be proved by small gain theorem. The simulation experiments can further demonstrate the good performance of the control method.

1. Introduction

For the Underactuated Underwater Vehicle (UUV), the path following control and the coordination control are two important problems. For the path following control problem, the path is in three-dimensional space. The virtual target points on the path are not constrained by time. A path can be represented by the mathematical expression: $P: s \rightarrow R^3, s \in [0, S], S \in R^+$, where s represents time. s is a independent path parameter. The control objective for the path following problem is that: the UUV can reach and follow a smooth given spacial path from a given initial state. When the UUV performs specific tasks in deep water, the linear path following control can no longer meet the task requirements. Therefore, we need to study the spacial curve path following control problem.

Many scholars are devoted to the research of the path following control method. In 2011, Lionel Lapierre proposed an improved method to generate a desired path. This method is based on Lyapunov stability theory and backstepping control technique. The efficiency of path following is improved by this method (Xiang et al., 2011). In the same year, Børhaug considered the problem of path following control for underactuated surface vessels with unknown ocean current disturbance. The proposed controllers are designed based on line-of-sight guidance, adaptive control, and cascaded systems theory. The controllers can drive the vessels to move along the desired paths. The formation control target is achieved by adjusting the vessels' speed (Børhaug et al., 2011). In 2012, Liljeback proposed a path following controller that enables snake robots to track straight paths. Using cascaded systems theory, the proposed path following controller is proved to be K-exponentially stable. The snake robot can move to any desired straight path under the assumption that the forward velocity is nonzero and positive (Liljeback et al., 2012). Zhi-Yong Liu proposed the path following algorithm to solve the matching problems on undirected graph models and exhibited a state-of-the-art performance on matching accuracy (Liu et al., 2012). In 2013, Dinh studied an inexact perturbed path-following algorithm in the framework of Lagrangian dual decomposition for solving large-scale separable convex programming problems. Unlike the exact versions considered in the literature, Dinh propose to solve the primal subproblems inexactly up to a given accuracy (Dinh et al., 2013). In the same year, Alessandretti addressed the design of model predictive control laws to solve the trajectory-tracking problem and the path-following problem for constrained underactuated

* Corresponding author.
E-mail addresses: qixuesnow@163.com (X. Qi), 1187615105@qq.com (P. Xiang), commandingo@163.com (Z.-j. Cai).

Peer review under responsibility of Society of Naval Architects of Korea.

https://doi.org/10.1016/j.ijnaoe.2019.11.003

vehicles. By allowing an arbitrarily small asymptotic tracking error, Alessandretti derive model predictive control laws. The size of the terminal error set is only limited by the size of the system constraints set (Alessandretti et al., 2013). In 2015, Fossen presented a nonlinear adaptive path-following controller that compensates for drift forces through vehicle sideslip. The proposed algorithm is motivated by a line of sight guidance principle used by ancient navigators, which is extended to path following of Dubins paths (Fossen et al., 2015). In paper (Kaminer et al., 2015), path following relies on the augmentation of existing autopilots with L1 adaptive output feedback control laws to obtain inner-outer loop control structures with guaranteed performance. In 2016, Faulwasser considered the tracking of geometric paths in output spaces of nonlinear systems subject to input and state constraints without prespecified timing requirements (Faulwasser and Findeisen, 2016). In 2017, Wen Xing designed the topology of leader-follower architecture as a combination of an undirected graph between followers and a digraph between leaders and followers (Xing et al., 2017).

The coordination control method of multiple UUVs is mainly divided into two types: analytic method and algorithmic method. Based on the mathematical tools, the analytic method rigorously analyzes coordination control behavior, including leader following strategy (Loria et al., 2016; Mariottini et al., 2015), virtual structure approach (Askari et al., 2015), artificial potential method (Ruchti et al., 2015), decentralized coordinated control (Li et al., 2010; Antonelli et al., 2014), and so on. In (Loria et al., 2016), Loria assumed that only one swarm leader robot has the information of the reference trajectory. The proposed controllers are partially linear time-varying. The main results ensure the uniform global asymptotic stabilization of the closed-loop system. In (Mariottini et al., 2015), Mariottini employed an Extended Kalman Filter for the estimation of each follower position and orientation with respect to the leader and adopted a feedback linearizing control strategy to achieve a desired formation. The leader follower formation control only need the leader's trajectory. And then, the whole robots will be controlled. Therefore, its formation control structure is simple and widely used. But there is no feedback from the followers to the leader. When the leader is disturbed, the whole system of the formation will likely collapse. In (Askari et al., 2015), a new formation flying approach based on virtual structure is presented. The control laws for formation control are designed based on both classical theory and inverse dynamics. The virtual structure method is easy to determine the formation behavior of the whole group. It is easy to maintain the formation. Because the formation feedback exists, it prevents the members from leaving the team. But the formation is required to remain in the same virtual structure, lacking flexibility and adaptability. When the formation needs to be changed, its application is greatly limited. In (Ruchti et al., 2015), artificial potential fields provide a computationally efficient solution to the problem of collision avoidance. The advantage of the artificial potential method is that: the algorithm is intuitive and effective, the calculation is simple and easy to realize real-time control. Especially, it can effectively deal with obstacle avoidance and collision avoidance with obstacle constraints. The shortcoming lies in the existence of the local minimum, so it is difficult to design the proper potential field function. In (Li et al., 2010), the control of multi-agent systems is considered as decentralized control and coordination of agents. In (Antonelli et al., 2014), the solution is proven to work in the case of strongly connected non-switching topologies and in the case of balanced strongly connected switching topologies.

The algorithm method does not require strict mathematical specifications, and mainly uses digital simulation to observe formation control behavior, such as behavior based formation control (Xu et al., 2014; Gao et al., 2012). In (Xu et al., 2014), a behavior-based control design approach is proposed for both efficient initial formation and formation control while avoiding obstacles. In (Gao et al., 2012), Five sub-behaviors called move-to-goal, avoid-obstacles, swirl-obstacle, keep-formation and random-noise were designed for the formation control mission. The behavior based formation method has the advantage that when the robot has multiple competing targets, it is easy to obtain the overall control strategy. Since the robot can sense the response according to the other robots' positions, there is a definite formation feedback in the system. In addition, the reactive behavior in the system can bring better real-time performance, and has some advantages in robot collision avoidance and obstacle avoidance. The main drawback is that the overall behavior of the formation can not be clearly defined, and it is difficult to analyze with accurate mathematical methods. The stability of the formation can not be guaranteed. In (Ghabcheloo et al., 2009), the coordinated path-following problem in the presence of communication losses and time delays is discussed. In (Bai et al., 2017), the distributed formation control of fractional-order multi-agent systems with absolute damping and communication delay is considered.

The coordinated formation control is generally divided into two types: leader-follower control and distributed control. For the leader-follower control, the leader robot should be controlled moving along a desired path. At the same time, the follower robots must maintain a desired geometric formation with the leader robot. The leader-follower control requires each follower communicate with the leader. Once the leader robot fails, it will lead to the failure of the formation control. For the distributed control, each robot has equal status. The robots can transmit information to each other. And then, a communication topology can be established. Under the communication topology, coordinated control laws are designed for each robot to achieve the formation objective. Distributed control can avoid formation failure caused by the broken leader in leader-follower control. The distributed control method is flexible. The formation convergence speed is fast for the distributed control. But there are also some shortcomings: the increase of communication, the increase of energy consumption of the system, and the stricter requirement of the distance between robots, and so on.

The early formation control of multiple UUVs requires only the relative position or distance information among multiple UUVs. The path of a single UUV wasn't restricted. When performing special tasks, such as subsea pipeline inspection, seabed maps' establishment, the UUV must follow a specified path. Obviously, the traditional formation controller can not solve such a special formation problem. On the basis of the above research work, combining path following and coordination control together, a new distributed controllers for formation control of multiple UUVs are proposed in this paper. The proposed controller can guarantee that each UUV moves on the desired path and the whole team maintain the required formation in three-dimensional space. The dynamic model of the UUV in three-dimensional space in (Jia, 2012) is used for reference. The time variation and boundedness of the hydrodynamic coefficients are sufficiently taken into account. In the aspect of the controller design, the path following control is carried out firstly, and then the speed is adjusted to achieve the formation requirement. Based on the Lyapunov theory and backstepping technique, the optimal motion planning problem is solved by the control method. From the actual situation of the UUV, the path following and the coordination control are implemented simultaneously. Based on the Lyapunov stability theory, the error signals of the path following and the coordination in the multiple UUVs' closed-loop system are proved asymptotically converge to zero. Finally, the simulation experiment proves the good effect of the control method.

The contributions of this paper are described as follows.

(1) The path following error dynamic system in three dimensional space is established in Serret-Frenet frame. Based on the line of sight navigation, the path following control law is designed. Moreover, the time variation and boundedness of hydrodynamic coefficients are fully taken into account. The designed path following controller can converge the path tracking error to zero asymptotically.
(2) Based on the graph theory, the algebraic expression of the coordination error dynamic system is given in this paper. And the coordinated control error converges to zero asymptotically by adjusting the speed of the UUV.
(3) The path following subsystem and the coordinated control subsystem are interconnected. Based on the small gain theory, it can be proved that the interconnected system is input-to-state stable.

The rest of the content of this paper is structured as follows: Section 2 presents the dynamic model of the i th UUV in three dimensional space. The path following controller for the i th UUV is introduced in Section 3. The coordinated controller for multiple UUVs is introduced in Section 4. Simulation experiment and analysis are introduced in Section 5. Section 6 summarizes and generalizes the full text.

2. Model description

In this section, the dynamic model of the i th UUV in three dimensional space is introduced.

Considering a group of n UUVs, Fig. 1 shows the path following reference frame of the i th UUV. $i = 1, 2, \cdots, n$. $\{U\}$ denotes the earth-fixed frame of all UUVs. $\{F_i\}$ and $\{B_i\}$ denote the Serret-Frenet frame and the body-fixed frame of the ith UUV respectively. Q_i is the centre of gravity for the i th UUV. Q_i is chosen to coincide with the origin Q_{B_i} of $\{B_i\}$. $[x_i, y_i, z_i]^{\mathrm{T}}$denotes the position of the point Q_i in $\{U\}$. $[\varphi_i, \theta_i, \psi_i]^{\mathrm{T}}$ denotes the orientation of the point Q_i in $\{U\}$. $[u_i, v_i, w_i]^{\mathrm{T}}$ is the vector of vehicle's velocities expressed in $\{B_i\}$. $[p_i, q_i, r_i]^{\mathrm{T}}$is the vector of vehicle's angular velocities expressed in $\{B_i\}$.

Define $\gamma_{Q_i} = \arctan(\dot{y}_i/\dot{x}_i)$ as the track angle, $\chi_{Q_i} = -\arctan(\dot{z}_i/\sqrt{\dot{x}_i^2 + \dot{y}_i^2})$ as the float angle, $\alpha_i = \arctan(w_i/u_i)$ as the attack angle, and $\beta_i = \arctan(v_i/\sqrt{u_i^2 + w_i^2})$ as the side-slip angle,

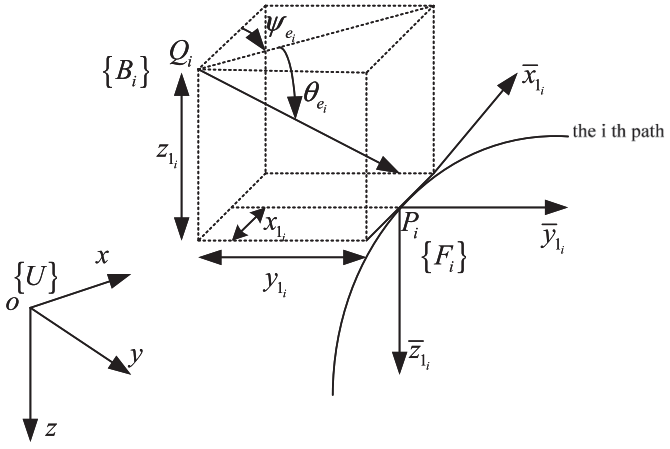

Fig. 1. Path-following reference frame for the ith UUV.

$u_i > 0$. Then the equations $\psi_i = \gamma_{Q_i} - \beta_i$ and $\theta_i = \chi_{Q_i} - \alpha_i$ are established. Let $\bar{v}_i = \sqrt{u_i^2 + v_i^2 + w_i^2}$ be the resultant velocity. The kinematic equations of the ith UUV could be modeled as follows (Jia, 2012):

$$\begin{aligned}
\dot{x}_i &= \bar{v}_i \cos\gamma_{Q_i} \cos\chi_{Q_i} \\
\dot{y}_i &= \bar{v}_i \sin\gamma_{Q_i} \cos\chi_{Q_i} \\
\dot{z}_i &= \bar{v}_i \sin\chi_{Q_i} \\
\dot{\chi}_{Q_i} &= q_i + \dot{\alpha}_i \\
\dot{\gamma}_{Q_i} &= \dot{r}_i/\cos\theta_i + \dot{\beta}_i
\end{aligned} \tag{1}$$

The dynamic model of the i th UUV is written in the actuated directions as follows:

$$\begin{aligned}
T_{x_i} &= m_{u_i}\dot{u}_i + d_{u_i} \\
0 &= m_{v_i}\dot{v}_i + m_{u_i r_i}u_i r_i + d_{v_i} \\
0 &= m_{w_i}\dot{w}_i + m_{u_i q_i}u_i q_i + d_{w_i} \\
M_{T_{z_i}} &= m_{r_i}\dot{r}_i + d_{r_i} \\
M_{T_{y_i}} &= m_{q_i}\dot{q}_i + d_{q_i}
\end{aligned} \tag{2}$$

where, $m_{u_i} = m_i - X_{\dot{u}_i}$, $m_{v_i} = m_i - Y_{\dot{v}_i}$, $m_{w_i} = m_i - Z_{\dot{w}_i}$, $m_{r_i} = I_{z_i} - N_{\dot{r}_i}$, $m_{q_i} = I_{y_i} - M_{\dot{q}_i}$ $m_{u_i r_i} = m_i - Y_{u_i r_i}$, $m_{u_i q_i} = m_i - Z_{u_i q_i}$, $d_{u_i} = -X_{u_i^2}u_i^2 - X_{v_i^2}v_i^2 - X_{w_i^2}w_i^2 - X_{q_i^2}q_i^2$, $d_{v_i} = -Y_{u_i v_i}u_i v_i - Y_{|v_i|v_i}|v_i|v_i$, $d_{w_i} = -Z_{u_i w_i}u_i w_i - Z_{|w_i|w_i}|w_i|w_i - m_i z_{g_i}q_i^2$,

$$d_{r_i} = -N_{u_i v_i}u_i v_i - N_{v_i|v_i|}v_i|v_i| - N_{u_i r_i}u_i r_i$$

$$d_{q_i} = -M_{q_i|q_i|}q_i|q_i| - M_{u_i q_i}u_i q_i - M_{u_i w_i}u_i w_i + (z_{g_i}W_i - z_{b_i}B_i)\sin\theta_i + m_i z_{g_i}(w_i q_i - v_i r_i)$$

where m_i and $m_{(\cdot)}$ are the mass and the associated mass of the i th UUV respectively. T_{x_i}, $M_{T_{z_i}}$ and $M_{T_{y_i}}$ are the torque signals respectively which are provided by the actuators. $X_{(\cdot)}$ $Y_{(\cdot)}$ $Z_{(\cdot)}$, $M_{(\cdot)}$ and $N_{(\cdot)}$ are the hydrodynamic coefficients respectively. $|v_i|v_i$, $|w_i|w_i$, $|q_i|q_i$ denote that their signs are determined by the direction of v_i, w_i, and q_i, and their size are proportional to v_i, w_i, and q_i. $I_{(\cdot)}$ is the moment of inertia. z_{g_i} is the centre of gravity's position in $\{B_i\}$. $z_{b_i}$is the centre of buoyancy's position in $\{B_i\}$. W_i and B_i are the gravity and the buoyancy of the i th UUV respectively.

Remark 1. In practical engineering applications, the response of the actuators and propellers is much more quickly than that of the UUV system. Therefore, their dynamics is reasonably neglected in this paper and their trivial effects are considered as unmodeled dynamics.

Assumption 1. The sway and the dive velocities of the ith UUV are passive-bounded in the sense that $|v_i| < B_{v_i}$ and $|w_i| < B_{w_i}$ where B_{v_i} and B_{w_i} are unknown constants.

Assumption 2. The position, orientation, and velocities of all UUVs in all degrees of freedom are available for feedback in real-time.

Remark 2. The velocity of a UUV is finite, so its components v_i and w_i are also bounded. In the controller designing process, it is reasonable to set the upper limits of v_i and w_i as finite constants. The UUV is usually equipped with position sensor, orientation sensor, and velocity sensor. And thus, we can receive these sensors' data in real time as inputs of the controllers. The sensors on the UUV can be used to sense the environment and their own state, but also to complete the corresponding oceanographic survey tasks.

3. Path following problem for the i th UUV

The i th UUV's motion model in $\{F_i\}$ -frame (Serret-Frenet frame) is studied in this section. $\{F_i\}$ -frame is defined based on the desired path. P_i is a arbitrary point on the i th desired path. The direction of $\bar{x}_{1_i}$ is the tangent direction of point P_i along the path. The direction of $\bar{y}_{1_i}$ is perpendicular to the direction of $\bar{x}_{1_i}$. Then there is $\bar{z}_{1_i}$ such that $\bar{z}_{1_i} = \bar{x}_{1_i} \times \bar{y}_{1_i}$. $P_i - \bar{x}_{1_i}\bar{y}_{1_i}\bar{z}_{1_i}$ is the $\{F_i\}$-frame. The coordinate of Q_i in $\{F_i\}$- frame is $[x_{1_i}, y_{1_i}, z_{1_i}]^{\mathrm{T}}$.

The kinematic equations of the ith UUV in $\{F_i\}$-frame could be modeled as follows (Jia, 2012):

$$\begin{aligned}
\dot{x}_{1_i} &= y_{1_i} c_{1_i}(s_i)\dot{s}_i - z_{1_i} c_{2_i}(s_i)\dot{s}_i + \bar{v}_i \cos\psi_{e_i} \cos\theta_{e_i} - \dot{s}_i \\
\dot{y}_{1_i} &= -x_{1_i} c_{1_i}(s_i)\dot{s}_i + \bar{v}_i \sin\psi_{e_i} \cos\theta_{e_i} \\
\dot{z}_{1_i} &= x_{1_i} c_{2_i}(s_i)\dot{s}_i - \bar{v}_i \sin\theta_{e_i} \\
\dot{\psi}_{e_i} &= r_i/\cos\theta_i + \dot{\beta}_i - c_{1_i}(s_i)\dot{s}_i \\
\dot{\theta}_{e_i} &= q_i + \dot{\alpha}_i - c_{2_i}(s_i)\dot{s}_i
\end{aligned} \tag{3}$$

where ψ_{e_i} and θ_{e_i} are orientation errors in $\{F_i\}$-frame. $c_{1_i}(s_i)$ and $c_{2_i}(s_i)$ are the path curvature. s_i is the parameter of the ith path. In general, s_i is the ith UUV's travel distance on the ith desired path.

In $\{F_i\}$-frame, P_i is an arbitrary point on the ith desired path. This breaks a strict constraint on the ith UUV's initial position. From Eq. (3), a kinematic controller is derived by adopting the angular speed r_i and q_i as virtual control inputs. The controller designed in Section 3.1 will drive errors x_{1_i}, y_{1_i}, z_{1_i}, ψ_{e_i} and θ_{e_i} to 0.

3.1. Path following controller based on the kinematic model of the ith UUV

This section derives a kinematic controller for the ith UUV. For moving on the desired path in a short time, we select line of sight angles for the ith UUV with the following form:

$$\delta_{\psi_{e_i}}(y_{1_i}) = \arcsin\left(-k_{1_i} y_{1_i} \Big/ \left(y_{1_i}^2 + \varepsilon_{1_i}\right)\right) \tag{4}$$

$$\delta_{\theta_{e_i}}(z_{1_i}) = \arcsin\left(k_{2_i} z_{1_i} \Big/ \left(z_{1_i}^2 + \varepsilon_{2_i}\right)\right) \tag{5}$$

where $k_{1_i} > 0$, $k_{2_i} > 0$, $\varepsilon_{1_i} > 0$ and $\varepsilon_{2_i} > 0$ are parameters of line of sight angles. $k_{1_i}^2 - 4\varepsilon_{1_i} \le 0$ and $k_{2_i}^2 - 4\varepsilon_{2_i} \le 0$ ensure the existence of the angles detailed in (4) and (5).

The ith path to be followed by the ith UUV is parameterized by its curvilinear abscissa s_i, and for each s_i the variables x_{1_i}, y_{1_i}, z_{1_i}, ψ_{e_i}, θ_{e_i}, c_{1_i} and c_{2_i} are well defined. The control laws are designed as follows:

$$r_i = \cos\theta_i\left(-k_{3_i}\left(\psi_{e_i} - \delta_{\psi_{e_i}}\right) - \dot{\beta}_i + c_{1_i}(s_i)\dot{s}_i + \dot{\delta}_{\psi_{e_i}}\right),\ k_{3_i} > 0 \tag{6}$$

$$q_i = -k_{4_i}\left(\theta_{e_i} - \delta_{\theta_{e_i}}\right) + c_{2_i}(s_i)\dot{s}_i + \dot{\delta}_{\theta_{e_i}} - \dot{\alpha}_i,\ k_{4_i} > 0 \tag{7}$$

$$\dot{s}_i = \bar{v}_i \cos\psi_{e_i} \cos\theta_{e_i} + k_{5_i} x_{1_i},\ k_{5_i} > 0 \tag{8}$$

Theorem 1. *The kinematic model of the ith UUV is expressed as* (1). *The path following error model in Serret-Frenet coordinate is expressed as* (3). *The line of sight angles are expressed as* (4) *and* (5). *For the ith given desired path S_i, choose control laws which are described in* (6), (7) *and* (8). *Then the tracking error $[x_{1_i}, y_{1_i}, z_{1_i}, \psi_{e_i}, \theta_{e_i}]^{\mathrm{T}}$ converges to $[0,0,0,0,0]^{\mathrm{T}}$ asymptotically for any initial position Q_i.*

Proof 1. *Firstly, consider a Lyapunov function candidate for the ith UUV*:

$$V_{1_i} = \left(\psi_{e_i} - \delta_{\psi_{e_i}}\right)^2 \Big/ 2 \tag{9}$$

The derivative of V_{1_i} is calculated as follows:

$$\begin{aligned}
\dot{V}_{1_i} &= \left(\psi_{e_i} - \delta_{\psi_{e_i}}\right)\left(\dot{\psi}_{e_i} - \dot{\delta}_{\psi_{e_i}}\right) \\
&= \left(\psi_{e_i} - \delta_{\psi_{e_i}}\right)\left(r_i/\cos\theta_i + \dot{\beta}_i - c_{1_i}(s_i)\dot{s}_i - \dot{\delta}_{\psi_{e_i}}\right)
\end{aligned} \tag{10}$$

By substituting (6) into (10), one obtains

$$\dot{V}_{1_i} = -k_{3_i}\left(\psi_{e_i} - \delta_{\psi_{e_i}}\right)^2 \le 0 \tag{11}$$

$V_{1_i}$is a positive monotone non increasing function whose upper bound is $\lim_{t\to\infty} V_{1_i} = \lim_{t\to\infty}(\psi_{e_i} - \delta_{\psi_{e_i}})^2/2 = l_{i_{\max}}$. $\ddot{V}_{1_i} = 2k_{3_i}^2(\psi_{e_i} - \delta_{\psi_{e_i}})^2 \ge 0$. The upper bound of $\ddot{V}_{1_i}$ is $\ddot{V}_{1_i} = 2k_{3_i}^2(\psi_{e_i} - \delta_{\psi_{e_i}})^2 = 4k_{3_i}^2 l_{i_{\max}}$. $\ddot{V}_{1_i}$ is bounded. Then $\dot{V}_{1_i}$ is uniformly continuous. Using Barbalat lemma, we can get:

$$\lim_{t\to\infty}\dot{V}_{1_i} = 0 \Rightarrow \lim_{t\to\infty}\psi_{e_i} = \lim_{t\to\infty}\delta_{\psi_{e_i}} \tag{12}$$

Secondly, consider a new Lyapunov function candidate:

$$V_{2_i} = \left(\theta_{e_i} - \delta_{\theta_{e_i}}\right)^2 \Big/ 2 \tag{13}$$

The derivative of V_{2_i} is calculated as follows:

$$\begin{aligned}
\dot{V}_{2_i} &= \left(\theta_{e_i} - \delta_{\theta_{e_i}}\right)\left(\dot{\theta}_{e_i} - \dot{\delta}_{\theta_{e_i}}\right) = \left(\theta_{e_i} - \delta_{\theta_{e_i}}\right) \\
&\times \left(q_i + \dot{\alpha}_i - c_{2_i}(s_i)\dot{s}_i - \dot{\delta}_{\theta_{e_i}}\right)
\end{aligned} \tag{14}$$

By substituting (7) into (14), one obtains

$$\dot{V}_{2_i} = -k_{4_i}\left(\theta_{e_i} - \delta_{\theta_{e_i}}\right)^2 \le 0 \tag{15}$$

Using Barbalat lemma ((Jia, 2012)), we can get:

$$\lim_{t\to\infty}\dot{V}_{2_i} = 0 \Rightarrow \lim_{t\to\infty}\theta_{e_i} = \lim_{t\to\infty}\delta_{\theta_{e_i}} \tag{16}$$

Under the guidance of the line of sight angle $\delta_{\psi_{e_i}}$ and $\delta_{\theta_{e_i}}$, the ith UUV's trajectory asymptotically converges to the invariant set:

$$\left\{\Omega_{1_i} \middle| (x_{1_i}, y_{1_i}, z_{1_i}) \in R^3, \psi_{e_i} = \delta_{\psi_{e_i}}, \theta_{e_i} = \delta_{\theta_{e_i}}\right\} \tag{17}$$

Therefore, x_{1_i}, y_{1_i}, z_{1_i}, ψ_{e_i}, and θ_{e_i} are bounded.

Thirdly, consider a new Lyapunov function candidate:

$$V_{3_i} = \left(x_{1_i}^2 + y_{1_i}^2 + z_{1_i}^2\right) \Big/ 2 \tag{18}$$

The derivative of V_{3_i} is calculated as follows:

$$\dot{V}_{3_i} = x_{1_i}\dot{x}_{1_i} + y_{1_i}\dot{y}_{1_i} + z_{1_i}\dot{z}_{1_i} = x_{1_i}\left(y_{1_i}c_{1_i}(s_i)\dot{s}_i - z_{1_i}c_{2_i}(s_i)\dot{s}_i + \bar{v}_i\cos\psi_{e_i}\cos\theta_{e_i} - \dot{s}_i\right) + y_{1_i}\left(\bar{v}_i\sin\psi_{e_i}\cos\theta_{e_i} - x_{1_i}c_{1_i}(s_i)\dot{s}_i\right) + z_{1_i}\left(x_{1_i}c_{2_i}(s_i)\dot{s}_i - \bar{v}_i\sin\theta_{e_i}\right) = x_{1_i}\bar{v}_i\cos\psi_{e_i}\cos\theta_{e_i} - x_{1_i}\dot{s}_i + y_{1_i}\bar{v}_i\sin\psi_{e_i}\cos\theta_{e_i} - z_{1_i}\bar{v}_i\sin\theta_{e_i} \tag{19}$$

By substituting (8) into (19), one obtains2

$$\begin{aligned}\dot{V}_{3_i} = & -k_{5_i}x_{1_i}^2 + y_{1_i}\bar{v}_i\sin\psi_{e_i}\cos\theta_{e_i} - z_{1_i}\bar{v}_i\sin\theta_{e_i} = -k_{5_i}x_{1_i}^2 + y_{1_i}\bar{v}_i\sin\delta_{\psi_{e_i}}\cos\delta_{\theta_{e_i}} - z_{1_i}\bar{v}_i\sin\delta_{\theta_{e_i}} \\ & = -k_{5_i}x_{1_i}^2 - k_{1_i}\bar{v}_i\cos\delta_{\theta_{e_i}}y_{1_i}^2\Big/\left(y_{1_i}^2+\varepsilon_{1_i}\right) - k_{2_i}\bar{v}_i z_{1_i}^2\Big/\left(z_{1_i}^2+\varepsilon_{2_i}\right)\end{aligned} \tag{20}$$

In general, $\theta_{e_i}\in(-\pi/2,\pi/2)$, so $\cos\theta_{e_i} = \cos\delta_{\theta_{e_i}} > 0$. From (20), we know that $\dot{V}_{3_i} \le 0$. $(x_{1_i}, y_{1_i}, z_{1_i}) = (0,0,0)$is the system equilibrium point. The system trajectory will asymptotically converge to the invariant set:

$$\left\{\Omega_{2_i}\middle|(x_{1_i},y_{1_i},z_{1_i}) = 0^3, \psi_{e_i} = \delta_{\psi_{e_i}}, \theta_{e_i} = \delta_{\theta_{e_i}}\right\} \tag{21}$$

Then the following results are deduced.

$$\lim_{t\to\infty}\psi_{e_i} = \lim_{t\to\infty}\delta_{\psi_{e_i}} = \lim_{t\to\infty}\arcsin\left(-k_{1_i}y_{1_i}\Big/\left(y_{1_i}^2+\varepsilon_{1_i}\right)\right) = 0 \tag{22}$$

$$\lim_{t\to\infty}\theta_{e_i} = \lim_{t\to\infty}\delta_{\theta_{e_i}} = \lim_{t\to\infty}\arcsin\left(k_{2_i}z_{1_i}\Big/\left(z_{1_i}^2+\varepsilon_{2_i}\right)\right) = 0 \tag{23}$$

The system trajectory will asymptotically converge to the invariant manifold $\{\Omega_{3_i}\big|(x_{1_i},y_{1_i},z_{1_i},\psi_{e_i},\theta_{e_i}) = 0^5\}$.

Finally, the first two steps show that under the effect of navigation control laws (6) and (7), each solution began in the set R^5asymptotically converges to the invariant set $\{\Omega_{1_i}\big|(x_{1_i}, y_{1_i}, z_{1_i})\in R^3, \psi_{e_i} = \delta_{\psi_{e_i}}, \theta_{e_i} = \delta_{\theta_{e_i}}\}$. The third step shows that under the effect of the tracking error control law (8), the system trajectory asymptotically converges to the invariant set$\{\Omega_{2_i}\big|(x_{1_i},y_{1_i},z_{1_i}) = 0^3, \psi_{e_i} = \delta_{\psi_{e_i}}, \theta_{e_i} = \delta_{\theta_{e_i}}\}$. Furthermore, we can prove that the largest invariant set of Ω_{2_i}practical equivalent to the set $\{\Omega_{3_i}\big|(x_{1_i},y_{1_i},z_{1_i},\psi_{e_i}, \theta_{e_i}) = 0^5\}$. By the LaSalle invariant set theory (Lapierre and Soetanto, 2007), the system trajectory will asymptotically converge to the largest invariant set $\{\Omega_{3_i}\big|(x_{1_i},y_{1_i},z_{1_i},\psi_{e_i},\theta_{e_i}) = 0^5\}$. This ends the Proof of Theorem 1. $(\psi_e - \delta), \varepsilon_1, (u-u_d), (\beta-\beta_d), \tilde{D}u$,

3.2. Path following controller based on the dynamic model of the ith UUV

The above feedback control laws apply to the kinematic model of the *i*th UUV only. In this section, using backstepping techniques, the control laws can be extended to deal with the *i*th UUV's dynamics. In section 3.1, the resultant velocity $\bar{v}_i$ of the *i*th UUV was left free, but it implicitly dependent on a desired speed $\bar{v}_{d_i}(s_i)$. In this section, the *i*th UUV's resultant velocity $\bar{v}_i$ is related to a desired speed $\bar{v}_{d_i}(s_i)$. Notice also that the *i*th UUV's angular speed r_i and q_i were assumed to be control inputs. The control problem is now transformed into the issue of designing control laws for system (1)–(3) with $M_{T_{z_i}}, M_{T_{y_i}}$, and T_{x_i} as the control inputs, so that $u_i \neq 0$ is guaranteed, and at the same time, $x_{1_i}(t)\to 0$, $y_{1_i}(t)\to 0$, $z_{1_i}(t)\to 0$, $\psi_{e_i}(t)\to 0$, $\theta_{e_i}(t)\to 0$, and $\bar{v}_i - \bar{v}_{d_i}(s_i)\to 0$ as $t\to\infty$. The control laws are designed as follows:

$$M_{T_{z_i}} = m_{r_i}\left(\cos\theta_i\left(-k_{3_i}\left(\dot{\psi}_{e_i} - \dot{\delta}_{\psi_{e_i}}\right) - \ddot{\beta}_i + c_{1_i}(s_i)\ddot{s}_i + \dot{c}_{1_i}(s_i)\dot{s}_i + \ddot{\delta}_{\psi_{e_i}}\right) - q_i\sin\theta_i\left(-k_{3_i}\left(\psi_{e_i} - \delta_{\psi_{e_i}}\right) - \dot{\beta}_i + c_{1_i}(s_i)\dot{s}_i + \dot{\delta}_{\psi_{e_i}}\right) - k_{6_i}\varepsilon_{r_i}\right) + d_{r_i} \tag{24}$$

$$M_{T_{y_i}} = m_{q_i}\left(\dot{c}_{2_i}(s_i)\dot{s}_i + c_{2_i}(s_i)\ddot{s}_i + \ddot{\delta}_{\theta_{e_i}} - \ddot{\alpha}_i - k_{4_i}\left(\dot{\theta}_{e_i} - \dot{\delta}_{\theta_{e_i}}\right) - k_{7_i}\varepsilon_{q_i}\right) + d_{q_i} \tag{25}$$

$$T_{x_i} = \left(v_i\left(m_{u_i r_i}u_i r_i + d_{v_i}\right)/\left(\bar{v}_i m_{v_i}\right) + w_i\left(m_{u_i q_i}u_i q_i + d_{w_i}\right)/\left(\bar{v}_i m_{w_i}\right) + \dot{\bar{v}}_{d_i}(s_i) - k_{8_i}\left(\bar{v}_i - \bar{v}_{d_i}(s_i)\right)\right)\cdot \bar{v}_i m_{u_i}/u_i + d_{u_i} \tag{26}$$

where $k_{6_i} > 0$, $k_{7_i} > 0$, $k_{8_i} > 0$.

Here, we give a reasonable Assumption 3. Under this assumption, the control input T_{x_i} designed in (26) is valid.

Assumption 3. If the initial velocity of the *i*th UUV is $u_i(0)\neq 0$, thus $T_{x_i}(0)\neq 0$. If there is a certain time t such that $u_i(t) = 0$, thus $T_{x_i}(t) = 0$.

The following result holds.

Theorem 2. *The kinematic model of the ith UUV is expressed as* (1).

The dynamic model of the ith UUV is expressed as (2). *The path following error model in Serret-Frenet coordinate is expressed as* (3). *The line of sight angles are expressed as* (4) *and* (5). *The speed tracking error is* $\bar{v}_i - \bar{v}_{d_i}(s_i)$, *where* $\bar{v}_{d_i}(s_i)$ *is the velocity changed with* s_i, *that is* $\dot{s}_i = \bar{v}_{d_i}(s_i)$. *The control laws are chosen as* (6), (7), (8), (24), (25) *and* (26). *Then, the path following errors of the ith UUV in the closed-loop system are tend to zero asymptotically.*

Proof 2. *Define the virtual control laws for* r_i *and* q_i *as follows*:

$$r_{1_i} = \cos\theta_i\Big(-k_{3_i}\Big(\psi_{e_i} - \delta_{\psi_{e_i}}\Big) - \dot{\beta}_i + c_{1_i}(s_i)\dot{s}_i + \dot{\delta}_{\psi_{e_i}}\Big) \tag{27}$$

$$q_{1_i} = -k_{4_i}\Big(\theta_{e_i} - \delta_{\theta_{e_i}}\Big) + c_{2_i}(s_i)\dot{s}_i + \dot{\delta}_{\theta_{e_i}} - \dot{\alpha}_i \tag{28}$$

Let $\varepsilon_{r_i} = r_i - r_{1_i}$ and $\varepsilon_{q_i} = q_i - q_{1_i}$ be the difference between the real values and the expected values of r_i and q_i respectively. Then

$$r_i = \varepsilon_{r_i} + r_{1_i} \tag{29}$$

$$q_i = \varepsilon_{q_i} + q_{1_i} \tag{30}$$

Consider the Lyapunov function as follows:

$$V_{4_i} = V_{3_i} + \varepsilon_{r_i}^2\Big/2 + \varepsilon_{q_i}^2\Big/2 + \left(\bar{v}_i - \bar{v}_{d_i}(s_i)\right)^2\Big/2 \tag{31}$$

The derivative of V_{4_i} is calculated as follows:

$$\dot{V}_{4_i} = \dot{V}_{3_i} + \varepsilon_{r_i}\Big(\Big(M_{T_{z_i}} - d_{r_i}\Big)\Big/m_{r_i} + q_i\sin\theta_i\Big(-k_{3_i}\Big(\psi_{e_i} - \delta_{\psi_{e_i}}\Big) - \dot{\beta}_i + c_{1_i}(s_i)\dot{s}_i + \dot{\delta}_{\psi_{e_i}}\Big) - \cos\theta_i\Big(-k_{3_i}\Big(\dot{\psi}_{e_i} - \dot{\delta}_{\psi_{e_i}}\Big) - \ddot{\beta}_i + c_{1_i}(s_i)\ddot{s}_i + \dot{c}_{1_i}(s_i)\dot{s}_i + \ddot{\delta}_{\psi_{e_i}}\Big)\Big) + \varepsilon_{q_i}\Big(\Big(M_{T_{y_i}} - d_{q_i}\Big)\Big/m_{q_i} + k_{4_i}\Big(\dot{\theta}_{e_i} - \dot{\delta}_{\theta_{e_i}}\Big) - \dot{c}_{2_i}(s_i)\dot{s}_i - c_{2_i}(s_i)\ddot{s}_i - \ddot{\delta}_{\theta_{e_i}} + \ddot{\alpha}_i\Big) + \left(\bar{v}_i - \bar{v}_{d_i}(s_i)\right)\cdot\left(u_i(T_{x_i} - d_{u_i})/(\bar{v}_i m_{u_i}) - v_i(m_{u_i r_i}u_i r_i + d_{v_i})/(\bar{v}_i m_{v_i}) - w_i(m_{u_i q_i}u_i q_i + d_{w_i})/(\bar{v}_i m_{w_i}) - \dot{\bar{v}}_{d_i}(s_i)\right) \tag{32}$$

By substituting (24), (25) and (26) into (32), one obtains

$$\dot{V}_{4_i} = -k_{5_i}x_{1_i}^2 - k_{1_i}\bar{v}_i\cos\delta_{\theta_{e_i}}y_{1_i}^2\Big/\Big(y_{1_i}^2 + \varepsilon_{1_i}\Big) - k_{2_i}\bar{v}_i z_{1_i}^2\Big/\Big(z_{1_i}^2 + \varepsilon_{2_i}\Big) - k_{6_i}\varepsilon_{r_i}^2 - k_{7_i}\varepsilon_{q_i}^2 - k_{8_i}\left(\bar{v}_i - \bar{v}_{d_i}(s_i)\right)^2$$

$$= -k_{5_i}x_{1_i}^2 - k_{9_i}y_{1_i}^2 - k_{10_i}z_{1_i}^2 - k_{6_i}\varepsilon_{r_i}^2 - k_{7_i}\varepsilon_{q_i}^2 - k_{8_i}\left(\bar{v}_i - \bar{v}_{d_i}(s_i)\right)^2 \tag{33}$$

where $k_{9_i} = k_{1_i}\bar{v}_i\cos\delta_{\theta_{e_i}}/(y_{1_i}^2 + \varepsilon_{1_i}) > 0$, $k_{10_i} = k_{2_i}\bar{v}_i/(z_{1_i}^2 + \varepsilon_{2_i}) > 0$. Then

$$\dot{V}_{4_i} \le -\lambda_i V_{4_i} \tag{34}$$

where $\lambda_i = 2\min\{k_{5_i}, k_{6_i}, k_{7_i}, k_{8_i}, k_{9_i}, k_{10_i}\}$. Then $x_{1_i}\to 0$, $y_{1_i}\to 0$, $z_{1_i}\to 0$, $\varepsilon_{r_i}\to 0$, $\varepsilon_{q_i}\to 0$ and $\bar{v}_i - \bar{v}_{d_i}(s_i)\to 0$ uniformly asymptotically. Combined with the control laws (6) and (7), the error signal $\psi_{e_i}\to 0$ and $\theta_{e_i}\to 0$ asymptotically. This ends the Proof of Theorem 2. *k*

At this stage, in preparation for the following sections, we state Theorem 3 on an asymptotically stable property that applies to a collection of the path following systems.

Theorem 3. *Consider a group of n UUVs. The path following subsystems satisfy the* Theorem 1 *and the* Theorem 2 *with* $\overline{X}_{PF} = [\overline{X}_i]_{6n\times 1}$, $\overline{X}_i = [x_{1_i}, y_{1_i}, z_{1_i}, \varepsilon_{r_i}, \varepsilon_{q_i}, \bar{v}_i - \bar{v}_{d_i}(s_i)]^{\mathrm{T}}$. *Then there exists a single Lyapunov function* V_{PF} *satisfying*: $V_{PF} > 0$, *and* $\dot{V}_{PF} \le -\lambda_{PF}V_{PF}$, *where* $\lambda_{PF} > 0$.

Proof 3. *choose a Lyapunov function for the ith UUV as follows*:

$$V_{4_i} = \overline{X}_i^{\mathrm{T}} I \overline{X}_i = \|\overline{X}_i\|^2\Big/2$$

where $I = diag[1,1,1,1,1,1]/2$. The derivative of V_{4_i} is calculated as follows:

$$\dot{V}_{4_i} \le -\lambda_i V_{4_i}$$

Choose a total Lyapunov function for a group of n UUVs as follows:

$$V_{PF} = \sum_{i=1}^{n} V_{4_i} = \|\overline{X}_{PF}\|^2\Big/2 > 0$$

The derivative of V_{PF} is calculated as follows:

$$\dot{V}_{PF} = \sum_{i=1}^{n}\dot{V}_{4_i} \le \sum_{i=1}^{n} -\lambda_i V_{4_i} = -\lambda_{PF}\sum_{i=1}^{n} V_{4_i} = -\lambda_{PF}V_{PF}$$

Then all the path following error signals of a group of n UUVs tend to zero uniformly asymptotically. This ends the Proof of Theorem 3. *k*

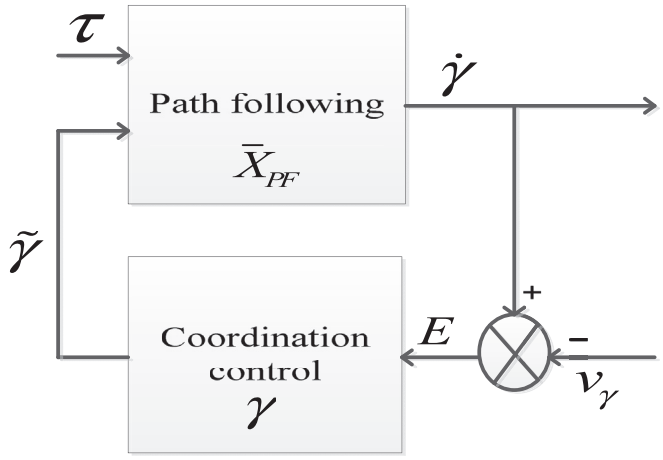

Fig. 2. The overall closed-loop system.

4. Coordination for multiple UUVs

If the path-following controller has been implemented for each UUV, that is, the ith UUV can move to the ith path from its initial position and travel along the ith path with velocity $\bar{v}_{d_i}(s_i)$. And now we should coordinate the entire group of multiple UUVs so as to achieve a desired formation pattern compatible with the paths adopted. This will be achieved by adjusting the desired speeds of the vehicles as functions of the along-path distances among them (Ghabcheloo et al., 2009).

Define $\gamma_i(s_i)$ as coordination state of the ith UUV. If $\gamma_i(s_i) - \gamma_j(s_j) = 0$, the multiple UUVs are coordinated. $i = 1, 2, \cdots, n, j \in N_i$ where N_i denotes the set of UUVs which the ith UUV communicates with. The formation speed tracking errors are defined as follows:$e_i = \dot{\gamma}_i - v_{\gamma_i}$ (35) where v_{γ_i} denotes a desired speed to be defined.

$$\dot{\gamma}_i = (d\gamma_i / ds_i) \cdot (ds_i / dt) = (d\gamma_i / ds_i) \cdot \bar{v}_{d_i} = v_{D_i} \tag{36}$$

where v_{D_i} is the coordination speed of the ith UUV. Let $\gamma = [\gamma_i]_{n\times 1}$, $v_\gamma = [v_{\gamma_i}]_{n\times 1}$, $E = [e_i]_{n\times 1}$, $\bar{v}_D = [v_{D_1}, \cdots, v_{D_n}]^T$.

The coordination control problem is described as follows: Consider the ith UUV, $i = 1, 2, \cdots, n$. Assume that γ_i and $\gamma_j, j \in N_i$, are available to the vehicle i. Derive a control law for v_{γ_i} such that $\lim_{t\to\infty}(\gamma_i - \gamma_j) = 0$, and the formation speed tracking errors $|\dot{\gamma}_i - v_{D_i}| \to 0$.

In order to solve the coordination control problem, the communication topology among the multiple UUVs must be modeled. We now recall some key concepts from algebraic graph theory and agreement algorithms and derive some basic tools that will be used in what follows.

4.1. Graph theory

Let $G(\upsilon, \text{ƛ})$ be the undirected graph induced by the multiple UUVs communication network, with υ denoting the set of n nodes and ƛ the set of edges. Nodes i and j are said to be adjacent if there is an edge between them. A path of length r between node i and node j consists of $r + 1$ consecutive adjacent nodes. We say that $G(\upsilon, \text{ƛ})$ is connected when there exists a path connecting every two nodes in the graph. The adjacency matrix of a graph, denoted A, is a square matrix with rows and columns indexed by the nodes such that the i,j-entry of A is 1 if $j \in N_i$ and zero otherwise. The degree matrix D of a graph $G(\upsilon, \text{ƛ})$ is a diagonal matrix where the i,i-entry equals $|N_i|$. $|N_i|$ is the cardinality of N_i. If $G(\upsilon, \text{ƛ})$ is connected, then $D^{-1}(D - A)$ is positive semi-definite. The Laplacian of a graph is defined as $L = D - A$. It is well known that L is symmetric and $L1 = 0$, where $1 = [1]_{n\times 1}$ and $0 = [0]_{n\times 1}$. If $G(\upsilon, \text{ƛ})$ is connected, then L has a simple eigenvalue at zero with an associated eigenvector 1, and the remaining eigenvalues are all positive.

Define the coordination error vector as follows:

$$\tilde{\gamma} = D^{-1}(D - A)\gamma \tag{37}$$

If $G(\upsilon, \text{ƛ})$ is connected, then $\text{rank}D^{-1}(D - A) = n - 1, D^{-1}(D - A) \cdot 1 = 0$, and

$$\tilde{\gamma} = 0 \Leftrightarrow \gamma_i = \gamma_j \Leftrightarrow \gamma \in span\{1\} \tag{38}$$

4.2. Coordination control of multiple UUVs

From (37), the evolution of the coordination error $\tilde{\gamma}$ is governed by

$$\dot{\tilde{\gamma}} = D^{-1}(D - A)\dot{\gamma} = D^{-1}(D - A)\bar{v}_D \tag{39}$$

We propose the following decentralized feedback law for the reference speeds v_γ as a function of the information obtained from the neighboring UUVs:

$$v_\gamma = \bar{v}_D + KD^{-1}(D - A)\gamma \tag{40}$$

where $K = diag[k_i] \in R_{n\times n}, k_i > 0, i = 1, 2, \cdots, n$. Using (39) and (40), the coordination dynamics take the form as follows:

$$\dot{\tilde{\gamma}} = D^{-1}(D - A)v_\gamma - D^{-1}(D - A)KD^{-1}(D - A)\gamma \tag{41}$$

That is $\dot{\tilde{\gamma}} = D^{-1}(D - A)v_\gamma - D^{-1}(D - A)K\tilde{\gamma}$. The control signals v_γ is viewed as disturbance, then$\tilde{\gamma} = 0$is the equilibrium point of closed-loop system $\dot{\tilde{\gamma}} = -D^{-1}(D - A)K\tilde{\gamma}$. And the equilibrium point is globally uniformly asymptotically stable.

Theorem 4. *Consider the coordination error dynamic system* (39) *with the decentralized feedback law* (40) *under the connected communication graph, then the coordination dynamic closed-loop system* (41) *is input-to-state stable.*

Proof 4. *Choose a Lyapunov function as follows*:

$$V_5 = \frac{1}{2}\tilde{\gamma}^T K^{-1}\tilde{\gamma} \tag{42}$$

compute the derivative of V_5 to obtain:

$$\dot{V}_5 = \tilde{\gamma}^T K^{-1}\dot{\tilde{\gamma}} = \tilde{\gamma}^T K^{-1}\left(D^{-1}(D-A)v_\gamma - D^{-1}(D-A)K\tilde{\gamma}\right) = \tilde{\gamma}^T K^{-1}D^{-1}(D-A)v_\gamma - \tilde{\gamma}^T D^{-1}(D-A)\tilde{\gamma}$$
$$= \tilde{\gamma}^T K^{-1}D^{-1}(D-A)v_\gamma - (1-\lambda+\lambda)\tilde{\gamma}^T D^{-1}(D-A)\tilde{\gamma} = -(1-\lambda)\tilde{\gamma}^T D^{-1}(D-A)\tilde{\gamma} + \tilde{\gamma}^T K^{-1}D^{-1}(D-A)v_\gamma - \lambda\tilde{\gamma}^T D^{-1}(D-A)\tilde{\gamma} \quad (43)$$

where $0<\lambda<1$, v_γ is bounded. Make k_i large enough to satisfy the following inequality:

$$\|\tilde{\gamma}\| \le \left\| v_\gamma K^{-1} \Big/ \lambda \right\| \quad (44)$$

Because $D^{-1}(D-A)$ is positive semidefinite, the following result is derived based on (43) and (44):

$$\dot{V}_5 \le -(1-\lambda)\tilde{\gamma}^T D^{-1}(D-A)\tilde{\gamma} \le 0 \quad (45)$$

That is $\dot{V}_5$ is negative semidefinite. From (44), we can get that $\|v_\gamma - \bar{v}_D\| \le \|v_\gamma\|/\lambda$. That is $\tilde{\gamma}$ is input-to-state stable with input signal v_γ. Then the coordination control closed-loop system of n UUVs is input-to-state stable. This ends the Proof of Theorem 4. *k*

Theorem 5. *Consider the interconnected system* $\sum$ *depicted in Fig. 2. For a group of n UUVs, the path following subsystems satisfy the Theorem 1, 2 and 3, and the coordination control subsystem satisfies the Theorem 4. Then,* $\sum$ *is input-to-state stable with respect to the states* $\tilde{\gamma}$ *and* $\bar{X}_{PF}$*, the input* τ*, where* $\tau = [\tau_1^{\mathrm{T}}, \cdots, \tau_n^{\mathrm{T}}]^{\mathrm{T}}$, $\tau_i = [T_{x_i}, M_{T_{y_i}}, M_{T_{z_i}}]^{\mathrm{T}}$, $i = 1, 2, \cdots, n$.

Proof 5. From Theorem 3, $\dot{V}_{PF} \le -\lambda_{PF}V_{PF}$, that is, for each $\eta_{PF} > 0$, there is $T(\eta_{PF}) > 0$ such that

$$\|\bar{X}_{PF}\| \le \eta_{PF},\ \forall t \ge t_0 + T(\eta_{PF}),\ \forall \|\bar{X}_{PF}\| < c_{PF} \quad (46)$$

From Theorem 4, there is a class KL function β_{CC} and a class K function γ_{CC} such that for any initial state $\tilde{\gamma}(t_0)$ and any bounded input v_γ, the solution $\tilde{\gamma}(t)$ exists for all $t \ge t_0$ and satisfies

$$\|\tilde{\gamma}(t)\| \le \beta_{CC}(\|\tilde{\gamma}(t_0)\|, t-t_0) + \gamma_{CC}\Big(\sup_{\tau_{CC}\ge t_0}\|v_\gamma(\tau_{CC})\|\Big),\ \forall t \ge t_0 \quad (47)$$

Using the input-to-state version of the small-gain theorem for the interconnection of (46) and (47), leads to the result. This ends the Proof of Theorem 5.

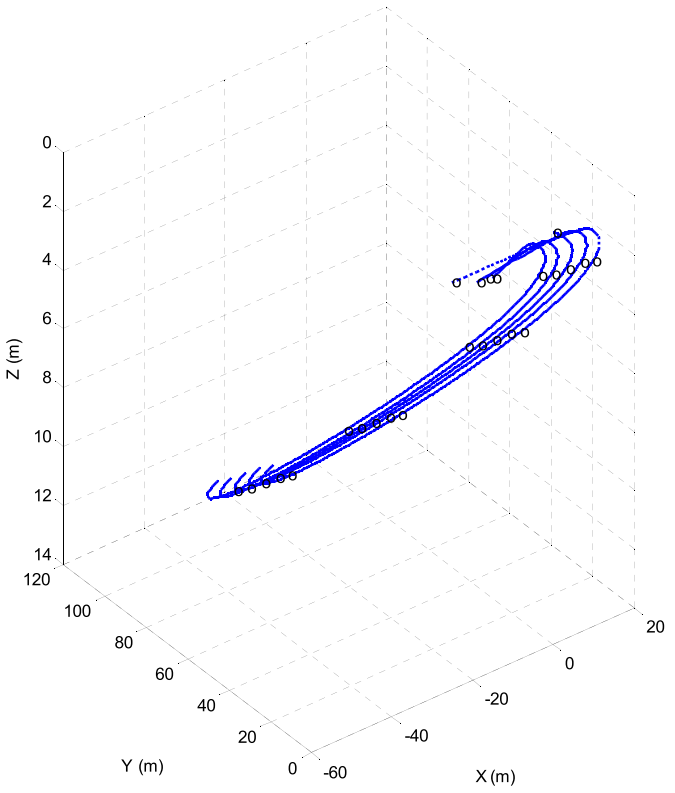

Fig. 3. The leader and followers trajectories.

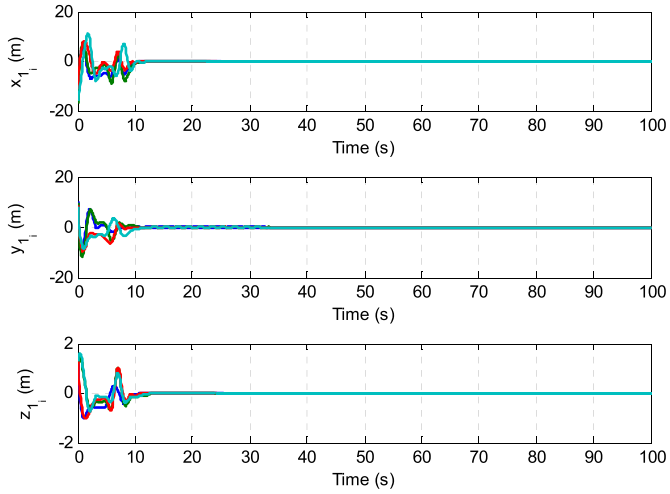

Fig. 4. Path following errors.

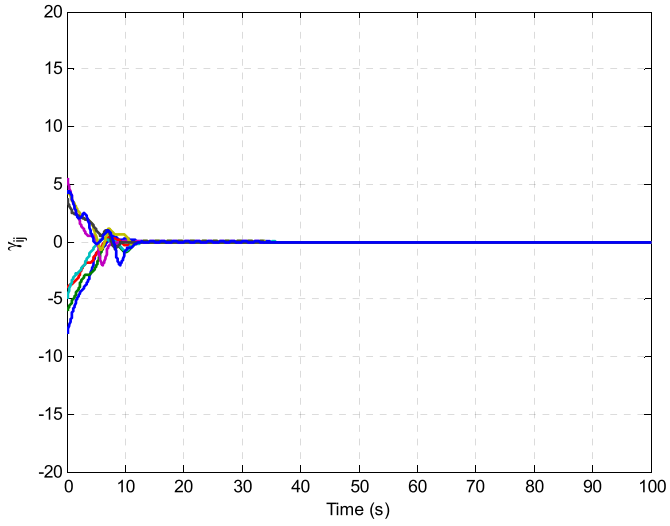

Fig. 5. Coordinate errors.

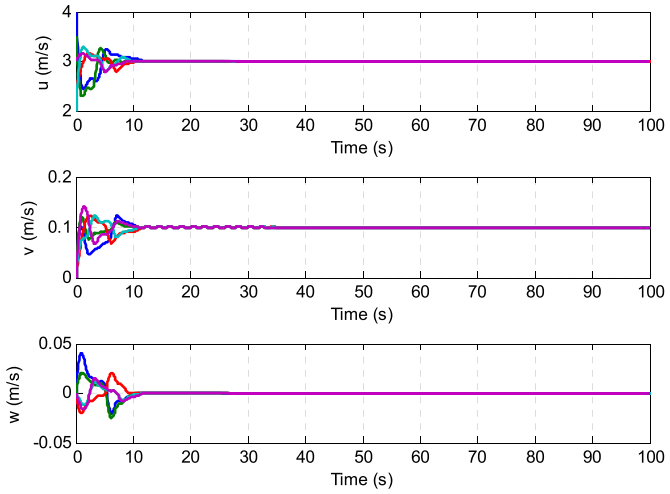

Fig. 6. The linear velocities of multiple UUVs.

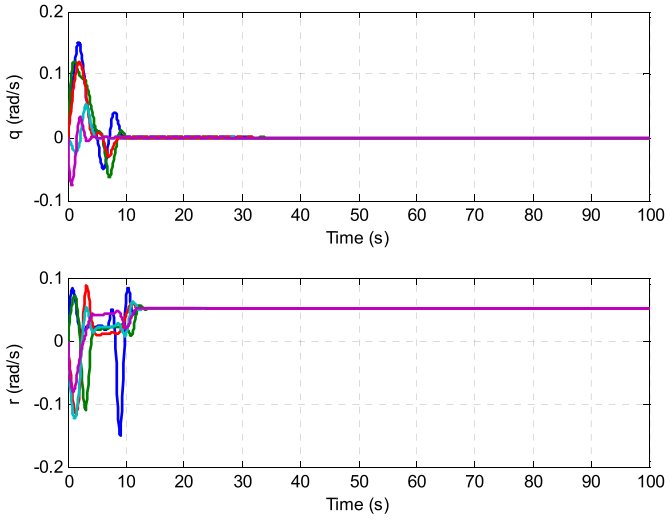

Fig. 7. The angular velocities of multiple UUVs.

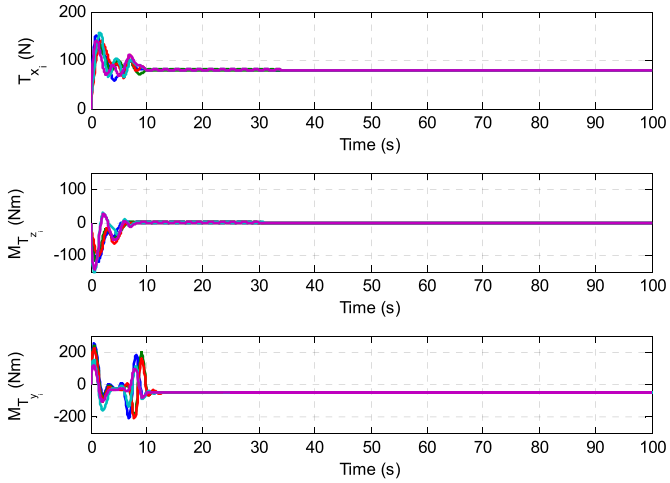

Fig. 8. Control signals.

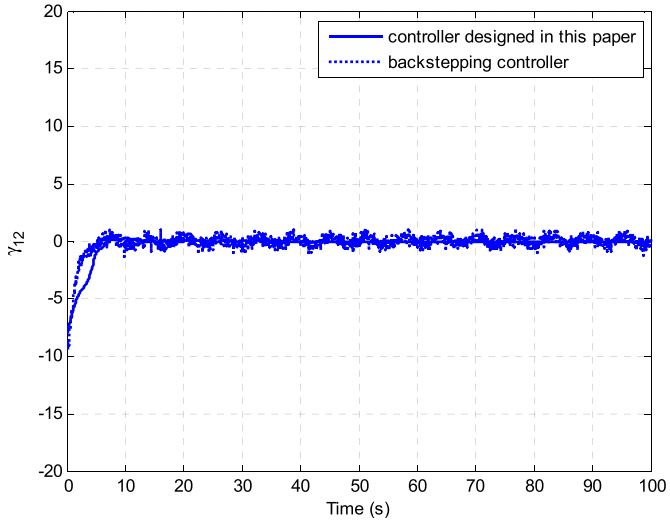

Fig. 9. Comparison of coordinate errors.

In the designing process of the controller, the controller $\tau_i = [T_{x_i}, M_{T_{y_i}}, M_{T_{z_i}}]^{\mathrm{T}}$ needs full state feedback of the system, including position, angle, linear velocity and angular velocity. In the process of coordinated control, the velocity of the UUV needs to be adjusted, which requires that the communication topology is interconnected. Therefore, it requires that the UUV be equipped with position sensor, orientation sensor, and velocity sensor.

On the basis of battery power, fuel battery, nuclear power, solar power and AIP power devices have been produced. Fuel batteries are characterized by high working current, high energy density, high energy efficiency, no pollution to the environment, and a life span of more than 10000 h. The fuel cylinder can not only provide buoyancy for UUV, but also be thrown away as an auxiliary fuel container. In the long run, fuel battery is a promising energy source. Lithium-ion batteries have the advantages of high voltage, high energy density, long cycle life, good safety, no pollution and low self-discharge rate. Lithium-ion batteries are likely to be an attractive alternative to UUV power sources. Many manufacturers are doing research in this area. Combined with various factors, a battery pack equipped with lithium-ion batteries is used here. For underwater vehicle projects, other possible options are either too expensive or important research projects in themselves. In addition, nuclear energy involves environmental and legal issues, which makes it impossible to be widely used in a short time.

5. Simulation analysis

To illustrate that the approach is applicable to UUV systems, simulation study is carried out based on a group of five UUVs. That is $i = 1, 2, 3, 4, 5$. Five UUVs must move along the desired spatial paths and keep the tangent slopes the same at the same time points.

The spatial paths for five UUVs are set to

$$\left[0.866t - \frac{t^2}{50} + \frac{t^3}{10^5} + \frac{t^4}{1.5\times 10^6}, \frac{t}{2} - \frac{t^2}{5\times 10^4} + \frac{t^3}{10^5} + \frac{t^4}{10^7}, \frac{t}{10}\right]$$

$$\left[0.866t-\frac{t^2}{50}+\frac{t^3}{10^5}+\frac{t^4}{1.5\times10^6}-7,\frac{t}{2}-\frac{t^2}{5\times10^4}+\frac{t^3}{10^5}+\frac{t^4}{10^7}-0.5,\frac{t}{10}-0.2\right]$$

$$\left[0.866t-\frac{t^2}{50}+\frac{t^3}{10^5}+\frac{t^4}{1.5\times10^6}+7,\frac{t}{2}-\frac{t^2}{5\times10^4}+\frac{t^3}{10^5}+\frac{t^4}{10^7}+0.5,\frac{t}{10}+0.2\right]$$

$$\left[0.866t-\frac{t^2}{50}+\frac{t^3}{10^5}+\frac{t^4}{1.5\times10^6}-4,\frac{t}{2}-\frac{t^2}{5\times10^4}+\frac{t^3}{10^5}+\frac{t^4}{10^7}-0.8,\frac{t}{10}-0.1\right]$$

$$\left[0.866t-\frac{t^2}{50}+\frac{t^3}{10^5}+\frac{t^4}{1.5\times10^6}+4,\frac{t}{2}-\frac{t^2}{5\times10^4}+\frac{t^3}{10^5}+\frac{t^4}{10^7}+0.8,\frac{t}{10}+0.1\right]$$

The initial positions of five UUVs are $[-20,10,1]$, $[-10,10,1.5]$, $[-15,8,1.2]$, $[-12,9,1.3]$ and $[0,0,0]$ respectively. The initial yaw angles of five UUVs are π, $\frac{5\pi}{6}$, $-\frac{2\pi}{3}$, 0 and $\frac{\pi}{6}$ respectively. The initial velocities are $u_1(0)=4(\mathrm{m/s})$, $u_2(0)=3.5(\mathrm{m/s})$, $u_3(0)=2.5(\mathrm{m/s})$, $u_4(0)=2(\mathrm{m/s})$, $u_5(0)=3(\mathrm{m/s})$, and $v_1(0)=v_2(0)=v_3(0)=v_4(0)=v_5(0)=0(\mathrm{m/s})$.

The initial angular velocities are

$$r_1(0)=r_2(0)=r_3(0)=r_4(0)=r_5(0)=0(\mathrm{rad/s})$$

The system parameters are selected as follows:

$$m_i=2234.5(\mathrm{kg}),\ X_{\dot{u}_i}=-142(\mathrm{kg}),\ Y_{\dot{v}_i}=-1715(\mathrm{kg}),\ Z_{\dot{w}_i}=2.0(\mathrm{kg}),$$
$$I_{Z_i}=2000\left(\mathrm{N\cdot m^2}\right),\ N_{\dot{r}_i}=-1350\left(\mathrm{N\cdot m^2}\right),\ I_{Y_i}=20\left(\mathrm{N\cdot m^2}\right),\ M_{\dot{q}_i}=7\left(\mathrm{N\cdot m^2}\right),$$
$$Y_{u_ir_i}=435(\mathrm{kg}),\ Z_{u_iq_i}=60(\mathrm{kg}),\ X_{u_i^2}=-35.4\left(\mathrm{kg\cdot m^{-1}}\right),\ X_{v_i^2}=-128.4\left(\mathrm{kg\cdot m^{-1}}\right),$$
$$X_{w_i^2}=-50.4\left(\mathrm{kg\cdot m^{-1}}\right),\ X_{q_i^2}=78.6\left(\mathrm{N\cdot m^{-1}}\right),\ Y_{u_iv_i}=-346\left(\mathrm{kg\cdot m^{-1}}\right),$$
$$Y_{|v_i|v_i}=-667\left(\mathrm{kg\cdot m^{-1}}\right),\ N_{u_iv_i}=-686(\mathrm{kg}),\ N_{|v_i|v_i}=443(\mathrm{kg}),\ N_{u_ir_i}=-1427(\mathrm{kg\cdot m}).$$

Controller parameters are selected as follows:

$$k_{1_i}=1,\ k_{2_i}=1,\ k_{3_i}=2,\ k_{4_i}=2,\ k_{5_i}=1,\ k_{6_i}=2,\ k_{7_i}=2,\ k_{8_i}=5,\ \varepsilon_{1_i}=1,$$
$$\varepsilon_{2_i}=1,\ N_1=\{5,4\},\ N_2=\{1,3\},\ N_3=\{5,2\},\ N_4=\{2,3\},\ N_5=\{1,4\},$$
$$K=\begin{bmatrix}10&0&0&0&0\\0&8&0&0&0\\0&0&5&0&0\\0&0&0&9&0\\0&0&0&0&6\end{bmatrix},\ A=\begin{bmatrix}0&0&0&1&1\\1&0&1&0&0\\0&1&0&0&1\\0&1&1&0&0\\1&0&0&1&0\end{bmatrix},\ D=\begin{bmatrix}2&0&0&0&0\\0&2&0&0&0\\0&0&2&0&0\\0&0&0&2&0\\0&0&0&0&2\end{bmatrix},$$
$$\gamma_i=\frac{ds_i}{dt},\ \bar{v}_D=[3\quad 3\quad 3\quad 3\quad 3]^{\mathrm{T}}$$

Fig. 3 shows the x-y-z plot of five UUVs trajectories. Fig. 4 shows the path following errors of five UUVs. Fig. 5 illustrates the evolution of the coordination errors. Clearly, five UUVs adjust their speeds to meet the formation requirements, and the coordination errors γ_{ij} converge to zero. The linear velocities and the angular velocities of the multiple UUVs are shown in Fig. 6 and Fig. 7 respectively. Fig. 8 shows the control signals of the multiple UUVs. In Fig. 9, a Gaussian white noise is added to the measured signals including position, orientation and velocities using randn($\cdot$) function to simulate real sensors. Fig. 9 shows the comparison of coordinate errors between the traditional backstepping

controller and the controller designed in this paper. From Fig. 9, we can see that the robustness of the proposed controller with respect to sensor failures is evident.

6. Conclusion

In the paper, the path following subsystem and the coordinated control subsystem are interconnected. In the path following subsystem, the control law is designed based on Lyapunov theory and backstepping technique. In the coordinated control subsystem, by adjusting the speed of the UUV, the coordination error tends to zero. Based on the small gain theory, the interconnected system is proved input-to- state stable. As far as the actual control effect is concerned, path following and coordinated motion are simultaneous. The effectiveness of the controller can be visualized by the simulation experiments.

In view of the complexity of the underwater working environment of multiple UUVs, the further work will be devoted to the research of obstacle avoidance, communication delay and energy saving.

Declaration of competing interest

The authors declare that they have no known competing financial interests or personal relationships that could have appeared to influence the work reported in this paper.

Acknowledgements

This work was supported by The training objects for young and middle-aged academic leaders in Anhui Science and Technology University in 2018, The 2017 National University Students' innovation and entrepreneurship training program (201710879049), and The National Natural Science Foundation of China (61702007).

References

Alessandretti, A., Aguiar, A.P., Jones, C.N., 2013. Trajectory-tracking and path-following controllers for constrained underactuated vehicles using Model Predictive Control. In: Control Conference. EUCA, pp. 1371–1376.

Antonelli, G., Arrichiello, F., Caccavale, F., et al., 2014. Decentralized time-varying formation control for multi-robot systems. Int. J. Robot Res. 33 (7), 1029–1043.

Askari, A., Mortazavi, M., Talebi, H.A., 2015. UAV formation control via the virtual structure approach. J. Aero. Eng. 28 (1), 04014047.

Bai, J., Wen, G., Rahmani, A., et al., 2017. Distributed formation control of fractional-order multi-agent systems with absolute damping and communication delay. Int. J. Contr. Autom. Syst. 15 (1), 85–94.

Børhaug, E., Pavlov, A., Panteley, E., et al., 2011. Straight line path following for formations of underactuated marine surface vessels. IEEE Trans. Contr. Syst. Technol. 19 (3), 493–506.

Dinh, Q.T., Necoara, I., Savorgnan, C., et al., 2013. An inexact perturbed path-following method for Lagrangian decomposition in large-scale separable convex optimization. SIAM J. Optim. 23 (1), 95–125.

Faulwasser, T., Findeisen, R., 2016. Nonlinear model predictive control for constrained output path following. IEEE Trans. Automat. Contr. 61 (4), 1026–1039.

Fossen, T.I., Pettersen, K.Y., Galeazzi, R., 2015. Line-of-sight path following for Dubins paths with adaptive side slip compensation of drift forces. IEEE Trans. Contr. Syst. Technol. 23 (2), 820–827.

Gao, Q., Pang, Y., Dong-Hao, L.V., 2012. Simulation on Behavior-Based Formation Control of Multi-Robot. Automation & Instrumentation.

Ghabcheloo, R., Aguiar, A.P., Pascoal, A., et al., 2009. Coordinated path-following in the presence of communication losses and time delays. SIAM J. Contr. Optim. 48 (1), 234–265.

Jia, H.M., 2012. Study of Spatial Target Tracking Nonlinear Control of Underactuated UUV Based on Backstepping. A Dissertation for the Degree of D.Eng. Harbin Engineering University.

Kaminer, I., Yakimenko, O., Dobrokhodov, V., et al., 2015. Coordinated path following for time-critical missions of multiple UAVs via L1 adaptive output feedback controllers. In: AIAA Guidance, Navigation and Control Conference and Exhibit, pp. 281–286.

Lapierre, Lionel, Soetanto, Didik, 2007. Nonlinear path-following control of an AUV. Ocean Eng. 34 (11–12), 1734–1744.

Li, H., Karray, F., Basir, O., et al., 2010. An optimization algorithm for the coordinated hybrid agent framework. Int. J. Robot Autom. 25 (1), 1730–1735.

Liljeback, P., Haugstuen, I.U., Pettersen, K.Y., 2012. Path following control of planar snake robots using a cascaded approach. IEEE Trans. Contr. Syst. Technol. 20 (1), 111–126.

Liu, Z.Y., Qiao, H., Xu, L., 2012. An extended path following algorithm for graph-matching problem. IEEE Trans. Pattern Anal. Mach. Intell. 34 (7), 1451–1456.

Loria, A., Dasdemir, J., Jarquin, N.A., 2016. Leader–follower formation and tracking control of mobile robots along straight paths. IEEE Trans. Contr. Syst. Technol. 24 (2), 727–732.

Mariottini, G.L., Pappas, G., Prattichizzo, D., et al., 2015. Vision-based localization of leader-follower formations. Decision and Control. In: 2005 and 2005 European Control Conference. Cdc-Ecc '05. IEEE Conference on. IEEE, pp. 635–640.

Ruchti, J., Senkbeil, R., Carroll, J., et al., 2015. Unmanned aerial system collision avoidance using artificial potential fields. J. Aero. Inf. Syst. 11 (3), 140–144.

Xiang, X., Lapierre, L., Liu, C., et al., 2011. Path tracking: combined path following and trajectory tracking for autonomous underwater vehicles. In: International Conference on Intelligent Robots and Systems. IEEE, pp. 3558–3563.

Xing, W., Zhao, Y., Karimi, H., 2017. Convergence analysis on multi-AUV systems with leader-follower architecture[J]. IEEE Access (99), 1-1.

Xu, D., Zhang, X., Zhu, Z., et al., 2014. Behavior-based formation control of swarm robots. Math. Probl Eng. (1), 1214–1225.